Search for T Violation in $K^+ \to \pi^0 \mu^+ \nu$ Decays

J. Imazato

Institute of Particle and Nuclear Physics, High Energy Accelerator Research Organization (KEK), Oho 1-1, Tsukuba, Ibaraki, 305-0801 Japan
jun.imazato@kek.jp

1 Introduction

Time reversal (T) symmetry has long been a subject of interest from pre-modern physics times, since it implies the reversibility of motion – for instance, an identical trajectory of an object when time runs back in classical mechanics. In modern quantum field theories it has received renewed attention as a discrete symmetry of space/time along with charge conjugation (C) and parity reflection (P) [1]. Although C and P are each maximally violated in weak interactions, T (and CP) is almost exact symmetry in all the interactions including the weak interaction. The violation of T would have a great impact [2] since it would mean that the physics laws in the time-reversed world are different from ours. T violation has also an important meaning in particle physics since it is equivalent to CP violation according to the CPT theorem. We can study the sources of CP violation which are necessary to explain the baryon asymmetry in the universe.

The transverse muon polarization (P_T) in $K \to \pi\mu\nu$ ($K_{\mu 3}$) decays with T-odd correlation was suggested by Sakurai [3] about 50 years ago to be a clear signature of T violation. Unlike other T-odd channels in, e.g., nuclear beta decays, P_T in $K_{\mu 3}$ has the advantage that the final state interactions (FSI), which may mimic T violation by inducing a spurious T-odd effect, are very small [4, 5]. This argument applies most particularly to $K^+_{\mu 3}$ decay with only one charged particle in the final state where the FSI contribution is only from higher order loop levels and is calculable. Thus, it is not surprising that over the last two decades, dedicated experiments have been carried out in search of non-zero P_T in $K_{\mu 3}$ decays [6]. An important feature of a P_T study is the fact that the contribution to P_T from the standard model (SM) is nearly zero ($\sim 10^{-7}$). Therefore, in a P_T search we are investigating new physics beyond the SM.

The most recent research of P_T has been performed at KEK as the E246 experiment. This experiment was carried out by an international collaboration whose core members continue the current J-PARC experiment. The E246

Imazato, J.: *Search for T Violation in* $\mathrm{K}^+ \to \pi^0\mu^+\nu$ *Decays.*
Lect. Notes Phys. **781**, 75–104 (2009)
DOI 10.1007/978-3-642-00961-7_4

result was consistent with no T violation but provided the world best limit of $P_T = -0.0017 \pm 0.0023\ (stat) \pm 0.0017\ (syst)$ [7] and constrained the parameter spaces of several contender models. It was, however, statistics limited, mainly due to insufficient accelerator beam intensity in spite of smaller systematic errors.

Now we intend to continue the P_T experiment further at J-PARC where higher accelerator beam intensity will be available and a higher experimental sensitivity is promised, in order to search for new physics beyond SM. We aim for a sensitivity of $\delta P_T \sim 10^{-4}$ [8].

2 $K^+ \to \pi^0 \mu^+ \nu$ Decay and Muon Transverse Polarization

2.1 $K^+ \to \pi^0 \mu^+ \nu$ Decay

The decay matrix element of the $K_{\mu 3}$ decay based on the V-A theory can be written as [9–12]

$$M = \frac{G_F}{2} \sin\theta_c \Big[f_+ \left(q^2\right) \left(p_K^\lambda + p_\pi^\lambda\right) + f_- \left(q^2\right) \left(p_K^\lambda - p_\pi^\lambda\right) \Big] \cdot \Big[\overline{u}_\nu \gamma_\lambda \left(1 - \gamma_5\right) v_\mu \Big], \tag{1}$$

with two form factors $f_+(q^2)$ and $f_-(q^2)$ of the momentum transfer squared to the lepton pair, $q^2 = (p_K - p_\pi)^2$. Here, G_F is the Fermi constant, θ_c the Cabibbo angle, p_K, p_π, p_μ, and p_ν are the four momenta of the kaon, pion, muon, and anti-neutrino, respectively. Using $p_K = p_\pi + p_\mu + p_\nu$, this amplitude can be rewritten as follows:

$$M = \frac{G_F}{2} \sin\theta_c f_+ \left(q^2\right) \Big[2 p_K^\lambda \cdot \overline{u}_\nu \gamma_\lambda \left(1 - \gamma_5\right) v_\mu + \left(\xi \left(q^2\right) - 1\right) m_\mu \overline{u}_\nu \left(1 - \gamma_5\right) v_\mu \Big], \tag{2}$$

where the parameter $\xi(q^2)$ is defined as $\xi(q^2) = f_-(q^2)/f_+(q^2)$. The first term of Eq. (2) corresponds to the vector (and axial vector) amplitude and the second term corresponds to the scalar (and pseudo-scalar) amplitude. The parameters f_- and f_+ depend on q^2 as $f_\pm(q^2) = f_\pm(0)[1 + \lambda_\pm(q^2/m_\pi^2)]$. Both f_+ and f_- can, in general, be complex. If time reversal (T) is a good symmetry, the parameter ξ is real. Any non-zero value of Imξ would imply T violation. As we show below, an experimentally observed T-violating muon polarization P_T is directly proportional to Imξ. The currently adopted values are $\lambda_+ = 0.0284 \pm 0.0027$, $\xi(0) = -0.14 \pm 0.05$, and $\lambda_- = 0$. The Dalitz distribution for $K_{\mu 3}$ decay is given by

$$\rho\left(E_\pi, E_\mu\right) \propto f_+^2 \left(q^2\right) \Big[A + B\xi \left(q^2\right) + C\xi^2 \left(q^2\right) \Big], \tag{3}$$

with

$$A = m_K \left(2E_\mu E_\nu - m_K E'_\pi\right) + m_\mu^2 \left(\frac{1}{4}E'_\pi - E_\nu\right), \tag{4a}$$

$$B = m_\mu^2 \left(E_\nu - \frac{1}{2}E'_\pi\right), \tag{4b}$$

$$C = \frac{1}{4}m_\mu^2 E'_\pi, \tag{4c}$$

$$E'_\pi = \left(m_K^2 + m_\pi^2 - m_\mu^2\right)/(2m_K) - E_\pi, \tag{4d}$$

where E_π, E_μ, and E_ν are the energies of the pion, muon, and neutrino in the kaon center-of-mass frame, and M_K, m_π, and m_μ the masses of the kaon, pion, and muon, respectively.

2.2 Transverse Polarization P_T

In three-body decays such as $K_{\mu 3}$, one defines three orthogonal components of the muon polarization vector: the longitudinal (P_L), normal (P_N), and transverse (P_T) as the components parallel to the muon momentum $\boldsymbol{p_\mu}$, normal to P_L in the decay plane, and normal to the decay plane, respectively. They are scalar products of the polarization vector ($\boldsymbol{\sigma}_\mu$) with three corresponding combinations of the unit momentum vector as follows:

$$P_L = \frac{\boldsymbol{\sigma}_\mu \cdot \boldsymbol{p}_\mu}{|\boldsymbol{p}_\mu|}, \tag{5a}$$

$$P_N = \frac{\boldsymbol{\sigma}_\mu \cdot \left(\boldsymbol{p}_\mu \times \left(\boldsymbol{p}_\pi \times \boldsymbol{p}_\mu\right)\right)}{|\boldsymbol{p}_\mu \times \left(\boldsymbol{p}_\pi \times \boldsymbol{p}_\mu\right)|}, \tag{5b}$$

$$P_T = \frac{\boldsymbol{\sigma}_\mu \cdot \left(\boldsymbol{p}_\pi \times \boldsymbol{p}_\mu\right)}{|\boldsymbol{p}_\pi \times \boldsymbol{p}_\mu|}. \tag{5c}$$

As can be seen, the P_T changes sign under the time reversal operation, thus making it a T-odd observable. Using the decay probability (Eq. (3)) one can write the muon polarization in the kaon rest frame as [9–12] $\boldsymbol{\sigma}_\mu = \boldsymbol{P}/|\boldsymbol{P}|$, where $\boldsymbol{P}$ is determined as follows:

$$\begin{aligned}\boldsymbol{P} = &\left\{a_1(\xi) - a_2(\xi)\left[(m_K - E_\pi) + (E_\mu - m_\mu)\left(\boldsymbol{p}_\pi \cdot \boldsymbol{p}_\mu\right)/|\boldsymbol{p}_\mu|^2\right]\right\}\boldsymbol{p}_\mu \\ &- a_2(\xi)\, m_\mu \boldsymbol{p}_\pi + m_K m_\mu \mathrm{Im}(\xi)\left(\boldsymbol{p}_\pi \times \boldsymbol{p}_\mu\right),\end{aligned} \tag{6}$$

with

$$a_1(\xi) = 2m_K^2\left[E_\nu + \mathrm{Re}\left(b\left(q^2\right)\right)\left(E_\pi^* - E_\pi\right)\right], \tag{7a}$$

$$a_2(\xi) = m_K^2 + 2\mathrm{Re}\left(b\left(q^2\right)\right) m_K E_\mu + |b\left(q^2\right)|^2 m_\mu^2, \tag{7b}$$

$$b\left(q^2\right) = \frac{1}{2}[\xi\left(q^2\right) - 1], \quad \text{and} \tag{7c}$$

$$E_\pi^* = \left(m_K^2 + m_\pi^2 - m_\mu^2\right)/(2m_K). \tag{7d}$$

One has to look for P_T in the presence of predominant in-plane components of the polarization P_L and P_N. P_T (Eq. (5)) can be further rewritten in terms of Imξ and a kinematical factor as follows:

$$P_T = \mathrm{Im}\xi \cdot \frac{m_\mu}{m_K} \frac{|\boldsymbol{p}_\mu|}{[E_\mu + |\boldsymbol{p}_\mu| \boldsymbol{n}_\mu \cdot \boldsymbol{n}_\nu - m_\mu^2/m_K]}. \tag{8}$$

The quantity Imξ, sensitive to the T violation, can thus be determined from a P_T measurement. The kinematic factor as a function of π^0 energy and μ^+ energy has an average value of $\sim$0.3 yielding a full detector acceptance relation of $< P_T > \sim 0.3\,\mathrm{Im}\xi$.

It is of interest to establish the connection between the Imξ and effective parameters of new physics appearing in the coefficients of generic exotic interactions. To this end, an effective four-fermion Lagrangian can be used:

$$\begin{aligned} L = & -\frac{G_F}{\sqrt{2}} \sin\theta_C\, \bar{s}\gamma_\alpha (1-\gamma_5)\, u\, \bar{\nu}\gamma^\alpha (1-\gamma_5)\, \mu \\ & + G_S\, \bar{s}u\, \bar{\nu}\, (1+\gamma_5)\, \mu + G_P\, \bar{s}\gamma_5 u\, \bar{\nu}\, (1+\gamma_5)\, \mu \\ & + G_V\, \bar{s}\gamma_\alpha u\, \bar{\nu}\gamma^\alpha (1-\gamma_5)\, \mu + G_A\, \bar{s}\gamma_\alpha\gamma_5 u\, \bar{\nu}\gamma^\alpha (1-\gamma_5)\, \mu + \mathrm{h.c.}, \end{aligned} \tag{9}$$

where G_S and G_P are the scalar and pseudo-scalar coupling constants and G_V and G_A are the exotic vector and axial vector coupling constants, respectively. Tensor interactions are neglected. Imξ is found to be caused only by the interference between the SM term and the scalar term, namely by the complex phase of G_S [13, 14], which can be written as

$$\mathrm{Im}\xi = \frac{\left(m_K^2 - m_\pi^2\right) \mathrm{Im}G_S^*}{\sqrt{2}\,(m_s - m_u)\, m_\mu G_F \sin\theta_C}, \tag{10}$$

where m_s and m_u are the masses of the s-quark and u-quark, respectively. Thus, P_T can constrain the exotic scalar interactions. The situation is different in the similar transverse muon polarization P_T in the radiative kaon decay $K^+ \to \mu^+\nu\gamma$, which is caused by pseudo-scalar interactions G_P [14].

2.3 P_T and CP Violation Beyond the Standard Model

P_T in the Standard Model

In order to formulate physics motivation for this experiment, we look first at what is predicted in the SM for P_T. A T-violating (or CP-violating) amplitude arises from the relative phases between diagrams or complex coupling constants in a diagram. Since only a single element of the CKM matrix V_{us} is involved for the W-exchanging semi-leptonic $K_{\mu 3}$ decay in the SM, no CP violation appears in the first order. As is discussed in [15] this is a general feature for vector (and axial vector)-type interactions. The SM contribution comes from only higher order effects. The possible size of its contribution was

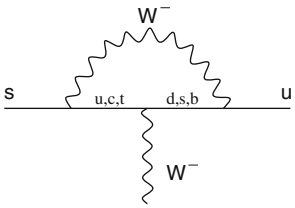

Fig. 1. Radiative corrections in the $K_{\mu 3}$ decay which provide a standard model contribution to P_T [1].

once suggested qualitatively in [16] to be $P_T < 10^{-6}$. An actual value based on the lowest order vertex radiative corrections to the $\bar{u}\gamma_\mu(1-\gamma_5)sW^\mu$ vertex (Fig. 1) was presented in the textbook of Bigi and Sanda [1]. This has been estimated to be less than 10^{-7}. This fact constitutes the main motivation of the physics background for P_T experiment as a search for new physics. Since the effect arising from FSI is known to be of the order of 10^{-5} [4, 5] and it is calculable, an observation of a non-zero P_T implies unambiguously the existence of CP violation mechanisms beyond the SM, namely new physics. Assuming 10^{-6} for the ability of the FSI estimation, there is a large window to explore from the current limit of $P_T \sim 10^{-3}$, while several new physics models allow the appearance of P_T in the ranges of 10^{-4}–10^{-3} level at any time (Fig. 2). This situation is very similar to the study of the neutron electric dipole moment (n-EDM) which is also a T violation quantity, in which the current experimental limit of $d_n = 3.1 \times 10^{-26} e$ cm [17] is slowly approaching the SM prediction of $d_n \sim 10^{-31} e$ cm.

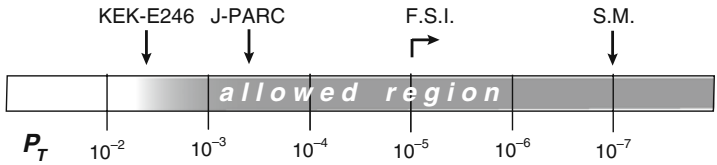

Fig. 2. Experimental status of $K_{\mu 3}$ P_T physics relative to the SM prediction is illustrated. The experimental limits are in 90% confidence limits. "Allowed region" means that some of the non-SM CP violation models allow $P_T < 10^{-2}$–10^{-3} without conflicting with other experimental limits.

2.4 CP Violation and Physics of P_T

Today there are intensive studies underway at accelerator laboratories searching for CP violation beyond the SM. In addition to the direct search for new particles at high-energy colliders, there are also many precision measurements to search for small deviations from the SM predictions. In B meson decays, e.g., the observation of a slight difference between the CP asymmetry of the $B \to J/\psi K_S^0$ process and that of the penguin diagram process [18] might be

a hint for new physics. In the kaon sector, the CP-violating $K_L \to \pi^0\nu\bar{\nu}$ rare decay study has been performed at KEK [19] and this will also be proposed at J-PARC. It is attempted to measure possible difference of the unitarity triangle from that of the B physics, but it can only be achieved with sufficient event statistics. Considering the current situation of our understanding of CP violation, the importance of a P_T search is increasing. There are several important characteristics of P_T physics. They are briefly summarized as follows:

- If P_T is found at the level of 10^{-4} which cannot be explained as FSI, it will correspond to "direct CP violation" in contrast to "indirect CP violation" due to the K_1^0–K_2^0 state mixing in the case of the K_0 system. The amount of direct CP violation in neutral kaons is found as the ratio $\varepsilon'/\varepsilon(\sim 10^{-3})$ which is consistent with SM predictions [20]. However, one should note that the agreement between the experiment and the theory, while good, still leaves large theoretical uncertainties. Therefore, the observation of CP violation in the charged kaon system is very much desired.
- Since the $K_{\mu 3}$ is a semi-leptonic process with W exchange in the SM resulting in a significant branching ratio, even a small amplitude of a new physics diagram with large mass scale can contribute to P_T through interference with this W exchange process with a consequence of a relatively large effect. (This is in strong contrast to new physics contribution to flavor changing neutral current rare decay processes in which the effect appears from loop diagrams.) In terms of the effective Lagrangian, $P_T \sim 1/\Lambda^2$ with the mass scale Λ, while the direct detection of rare decays, such as $K_L^0 \to \pi^0\nu\bar{\nu}$, should scale as $1/\Lambda^4$.
- Since the three Higgs doublets may allow a sizable value [21, 22], P_T can probe CP violation through the Higgs sector, of which, however, very little is known with regard to the structure and dynamics [1]. There is no constraint even on the number of Higgs doublets so far inferred theoretically. Models with an extended Higgs sector with more than one SM Higgs doublet allow many new sources of CP violation.
- If LHC finds the charged Higgs boson, the P_T measurement will become even more important to look for associated CP-violating couplings. It is expected that an MSSM Higgs boson should be discovered with 5σ significance after an integrated luminosity of 30 fb^{-1} if the condition of $\tan\beta/m_{H^+} \geq 0.06$ (GeV)$^{-1}$ is satisfied. If this limit is applied to the lightest charged Higgs boson in the context of the multi-Higgs model, the P_T corresponds to $|P_T| < 3 \times 10^{-4}$. This roughly corresponds to the aim of the J-PARC experiment of δP_T (one σ limit) $\sim 10^{-4}$.

2.5 Theoretical Models for P_T

In this section we briefly describe a few models which might lead to a sizable P_T value. We also give a more general discussion based on the effective field theory to clarify the difference of P_T physics from other T- and CP-violating observables.

Multi-Higgs Doublet Model

As the minimum and natural extension of the SM with one Higgs doublet, multi-Higgs doublet models have been considered, and a number of papers [21–29] have applied this model to P_T as one of the promising candidate theories. In the class of models without tree-level flavor changing neutral current, new CP-violating phases are introduced in the charged Higgs mass matrix if the number of doublets is more than 2. The coupling of quarks and leptons to the Higgs boson is expressed in terms of the Lagrangian [21, 22]:

$$L = \left(2\sqrt{2}G_F\right)^{\frac{1}{2}} \sum_{i=1}^{2} \{\alpha_i \bar{u_L} V M_D d_R H_i^+ + \beta_i \bar{u_R} M_U V d_L H_i^+ + \gamma_i \bar{\nu_L} M_E e_R H_i^+\} + \text{h.c.}, \tag{11}$$

where M_D, M_U, M_E are diagonal mass matrices, V is the CKM matrix, and α_i, β_i, and γ_i are the new complex coupling constants associated with the charged Higgs interactions. For the three-doublet case a natural flavor conservation can be arranged. The coefficients α_i, β_i, and γ_i can have complex phases, and P_T is calculated as follows:

$$\text{Im}\xi = \frac{m_K^2}{m_H^2} \text{Im}\left(\gamma_1 \alpha_1^*\right), \tag{12}$$

where α_1 and γ_1 are the quark and lepton couplings to the lightest charged Higgs boson (Fig. 3). The E246 result [8] yielded $|\text{Im}(\gamma_1 \alpha_1^*)| < 0.066(m_H/\text{GeV})^2$ as the most stringent limit for this parameter. $(\gamma_1 \alpha_1^*)$ is also constrained by the semi-leptonic decay of the B meson $B \to \tau \nu X$ [30, 31] as the deviation from the SM value, but the constraint on $|\text{Im}(\gamma_1 \alpha_1^*)|$ is less stringent than the P_T constraint. The recent observation of $B \to \tau \nu$ [32] constrains the model in a similar manner [33] but less stringent at the moment. Other constraints to this model come from the neutron EDM (d_n) [17], $b \to s\gamma$ [30, 31], and $b \to sl\bar{l}$ [34] complementing the P_T result in a different manner, since these channels limit $\text{Im}(\alpha_1 \beta_1^*)$. These two parameters are related as $\text{Im}(\alpha_1 \beta_1^*) = -(v_3/v_2)^2 \text{Im}(\gamma_1 \alpha_1^*)$ through the ratio of the Higgs field vacuum expectation values v_2 and v_3. An interesting scenario assumed in [21] is $v_2/v_3 \sim m_t/m_\tau \sim 95$, thus making P_T the most sensitive test of the three Higgs doublet model over d_n and $b \to s\gamma$ (Fig. 4).

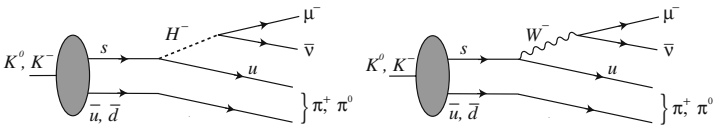

Fig. 3. P_T appears as the interference of the charged Higgs boson exchange with the standard model W boson exchange.

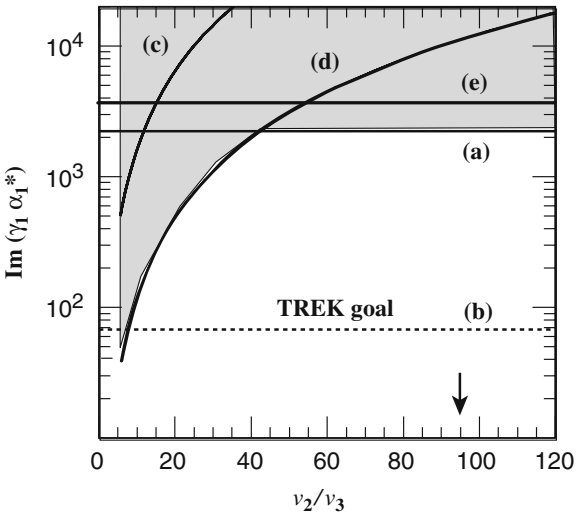

Fig. 4. Constraint to the three Higgs doublet model parameters of $|\mathrm{Im}(\gamma_1\alpha_1^*)|$ and v_2/v_3, the ratio of Higgs field vacuum expectation values, with the assumption of $m_{H^+} \cong 2m_Z$: (**a**) the P_T limit from the E246 experiment, (**b**) P_T expectation in TREK, (**c**) neutron electric dipole moment (EDM) only with the d-quark contribution, (**d**) $b \to s\gamma$, and (e) $b \to X\tau\nu$. The *gray region* is the excluded region. The *arrow* shows the most probable point of v_2/v_3 to be $m_t/m_\tau = 95$.

SUSY Models

A number of other models also allow P_T at observable level without conflicting with other experimental constraints. In other words, non-observation of P_T can constrain those models. Some models of minimal supersymmetric standard models (MSSM) allow sizable values. One interesting case is the model discussed by Wu and Ng [35]. In this model the complex coupling constant between the charged Higgs boson and strange- and up-quarks is induced through squark and gluino loops. Then, the P_T value when the muon and neutrino momenta are at right angles is given as

$$P_T^{H^+} \approx 3.5 \times 10^{-3} I_{H^+} \frac{p_\mu}{E_\mu} \frac{(\mu + A_t \cot\beta)}{m_g} \times \frac{(100\ \mathrm{GeV})^2}{M_H^2} \frac{\mathrm{Im}[V_{33}^{H^+} V_{32}^{D_L^*} V_{31}^{U_R^*}]}{\sin\theta_c} \tag{13}$$

for $\tan\beta \approx 50$. (For the meanings of various symbols, see Ref. [35] except to note that we assumed the top quark mass to be 180 GeV.) If we allow large flavor mixing coupling in the squark–quark vertices, there is an allowed parameter region for large P_T. The E246 P_T upper bound corresponds to $M_H > 140$ GeV. In view of several assumptions made, this bound should be

considered as a qualitative estimate [36]. It is noteworthy that $P_T(K_{\mu 3})$ and $P_T(K_{\mu\nu\gamma})$ have opposite signs in this model.

Although MSSM predicts only unobservably small P_T [37] without tuning of relevant flavor parameters, the SUSY with R-parity violation [36] can give rise to a sizable value of P_T. If R-parity violation is allowed, a superpotential is defined [38] as $W = W_{MSSM} + W_{RPV}$ with

$$W_{RPV} = \lambda_{ijk} L_i L_j \bar{E}_k + \lambda'_{ijk} L_i Q_j \bar{D}_k + \lambda''_{ijk} \bar{U}_i \bar{D}_j \bar{D}_k, \tag{14}$$

where $i, j = 1, 2, 3$ are generation indices with a summation implied. $L_i(Q_i)$ are the lepton (quark) doublet superfields and $\bar{E}_j(\bar{D}_j, \bar{U}_j)$ are the electron (down- and up-quark) singlet superfields. λ, λ', and λ'' are the Yukawa couplings; the former two relevant to lepton number violation and the latter relevant to baryon number violation. There are altogether 48 independent λ_{ijk}s which should be determined experimentally.

Our P_T can be expressed in this formalism as a sum of two components of slepton exchange and down-type squark exchange as $\mathrm{Im}\xi = \mathrm{Im}\xi^{\tilde{l}} + \mathrm{Im}\xi^{\tilde{d}}$ with

$$\mathrm{Im}\xi^{\tilde{l}} = \sum_i \frac{\mathrm{Im}[\lambda_{2i2} \left(\lambda'_{i12}\right)^*]}{4\sqrt{2} G_F \sin\theta_c \left(m_{\tilde{l}_i}\right)^2} \cdot \frac{m_K^2}{m_\mu m_s}, \tag{15a}$$

$$\mathrm{Im}\xi^{\tilde{d}} = \sum_i \frac{\mathrm{Im}[\lambda'_{21k} \left(\lambda'_{22k}\right)^*]}{4\sqrt{2} G_F \sin\theta_c \left(m_{\tilde{d}_k}\right)^2} \cdot \frac{m_K^2}{m_\mu m_s}. \tag{15b}$$

Thus, we constrain $\mathrm{Im}[\lambda_{2i2}(\lambda'_{i12})^*]/m^2_{\tilde{l}_i}$ and $\mathrm{Im}[\lambda'_{21k}(\lambda'_{22k})^*]/m^2_{\tilde{d}_k}$ (summation is implied). The E246 limit corresponds to 1.8×10^{-8} for these quantities, which will be improved by a factor of 20 at J-PARC. There are a number of experimental and theoretical efforts to analyze λ, λ', and λ'' in other channels. In a recent paper [39] and review papers [40, 41] currently updated limits are compiled also for the products $\lambda\lambda'$, $\lambda'\lambda'$, etc. There are six relevant parameters for P_T as shown in Eq. (15) which are summarized in Table 1.

Table 1. The R-parity violating SUSY parameters relevant to P_T and the constraints from other experiments.

	Parameter	Upper bound	Experiment
$\mathrm{Im}\xi^{\tilde{l}}$	$\lvert\lambda^*_{232}\lambda'_{312}\rvert$	$3.8 \times 10^{-6}\mathrm{m}^2$	$K_L \to \mu^+\mu^-$ [41]
	$\lvert\lambda^*_{212}\lambda'_{112}\rvert$	No constraint	
	$\lvert\lambda^*_{222}\lambda'_{212}\rvert$	No constraint	
$\mathrm{Im}\xi^{\tilde{d}}$	$\lvert\lambda'^*_{211}\lambda'_{221}\rvert$	$2.8 \times 10^{-5}\mathrm{m}^2$	$K^+ \to \pi^+\nu\bar{\nu}$ [42]
	$\lvert\lambda'^*_{212}\lambda'_{222}\rvert$	$2.8 \times 10^{-5}\mathrm{m}^2$	$K^+ \to \pi^+\nu\bar{\nu}$ [42]
	$\lvert\lambda'^*_{213}\lambda'_{223}\rvert$	$2.8 \times 10^{-5}\mathrm{m}^2$	$K^+ \to \pi^+\nu\bar{\nu}$ [42]

3 Experimental Status of P_T

3.1 Early Experiments

The measurement of P_T in $K_{\mu 3}$ decays has a long history. Early measurements of P_T were carried out at the Bevatron [43, 44] and Argonne [45] in $K^0_{\mu 3}$ decays but they lacked statistical significance. More advanced experiments prior to our work were done at the 28-GeV AGS at the Brookhaven National Laboratory (BNL). Morse et al. [46] measured P_T of muons from in-flight decay of $K^0_{\mu 3}$. From a data sample of 12 million events, they deduced $\mathrm{Im}\xi = 0.009 \pm 0.030$. This result, while consistent with zero, has a central value compatible with a prediction of 0.008, from the T-conserving final state interactions. As mentioned above, the final state interactions in $K^0_{\mu 3}$ decays obscure the real value of P_T. At the same facility, Blatt et al. [6] measured P_T of $K^+_{\mu 3}$ for the first time by detecting neutral particles from the in-flight decay of an unseparated 4 GeV/c K^+ beam. From a data sample of 21 million events, they deduced $\mathrm{Im}\xi = -0.016 \pm 0.025$, consistent with T invariance. The most recent result was from the KEK-PS E246 experiment [7] on which the current J-PARC experiment is based. The details of this experiment are presented next. Table 2 presents the world data as of today.

Table 2. Early experiments and their $\mathrm{Im}\xi$ results.

Laboratory	Decay	Year	$\mathrm{Im}\xi$	Ref.
Bevatron	$K^0_{\mu 3}$	1967	-0.02 ± 0.08	[43, 44]
Argonne	$K^0_{\mu 3}$	1973	-0.085 ± 0.064	[45]
BNL-AGS	$K^0_{\mu 3}$	1980	0.009 ± 0.030	[46]
BNL-AGS	$K^+_{\mu 3}$	1983	-0.016 ± 0.025	[6]
KEK-PS	$K^+_{\mu 3}$	2004	-0.005 ± 0.008	[7]

3.2 KEK E246 Experiment

The most recent and highest precision experiment was performed at the KEK proton synchrotron. The experiment used the stopped K^+ beam at the K5 low-momentum beam channel [47] with the superconducting toroidal spectrometer [48] setup. An elaborate detector (Fig. 5) consisting of a large-acceptance CsI(Tl) barrel, tracking chambers, an active target, and muon polarimeters was constructed and the data were taken between 1996 and 2000 for a total of 5,200 hours of beam time. A precise field mapping was made [49] before the measurements. Since K5 was equipped only with a single stage of electrostatic separator, the channel provided a beam with substantial π^+ contamination with a π/K ratio of about 8 for a 660 MeV/c beam.

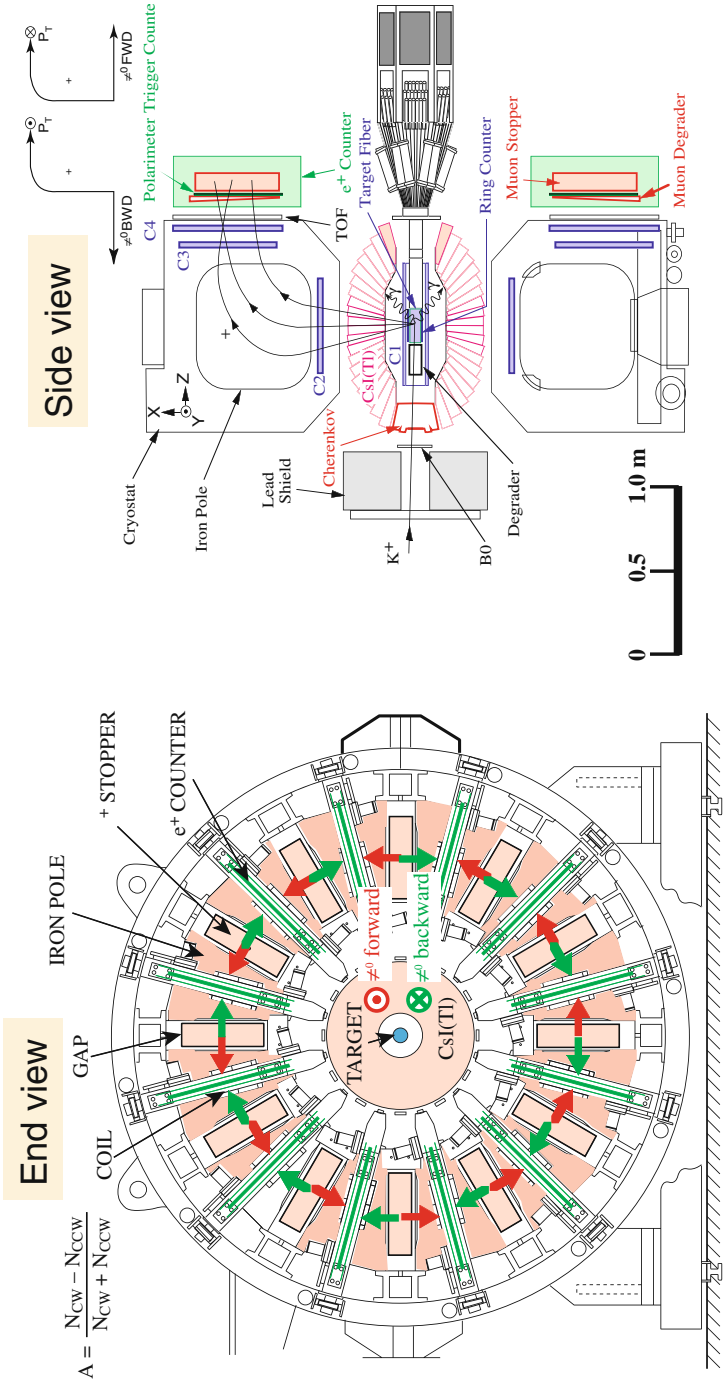

Fig. 5. Toroidal magnet setup for the TREK experiment.

Table 3. Experimental condition of E246.

Parameter	Value	Expectation at J-PARC
K^+ beamline	K5 with 660 MeV/c	K0.8 with 800 MeV/c
Proton intensity	1.0×10^{12}/s	0.54×10^{14}/s
K^+ beam intensity	1.0×10^5/s	2×10^6/s
π/K ratio	$\sim$8	<0.5
Beam duty factor	0.7 s/2.0 s	$>$0.7 s/3.5 s
Net runtime	$\sim$5200 hours (1.8×10^7s)	1.0×10^7s

(At J-PARC we expect $\pi/K < 0.5$.) The performance of the CsI(Tl) calorimeter was limited by this π^+ contamination with a halo resulting in accidental hits. The relatively low K^+ intensity of typically 10^5/s was the consequence of the maximum available proton beam intensity of 10^{12}/s from the slow extraction of the accelerator. The main parameters of the experiment are summarized in Table 3. Current estimates of these parameters at J-PARC are also shown.

The details of the detector were presented in [50]. Also, some individual elements have been documented in the literature, e.g., the CsI(Tl) calorimeter [51], its readout electronics [52], and the target ring counter system [53]. The features of the $K_{\mu 3}$ detection are (1) μ^+ (charged particle) detection by means of a tracking system with 3 MWPC and a fiber bundle target with the momentum analysis by the toroidal spectrometer and (2) π^0 detection as two photons or one photon with relatively large energy by the CsI(Tl) calorimeter. The muon polarization measurement relied on the sensitivity of the decay positron emission asymmetries in a longitudinal magnetic field with $< \mathbf{B} > \| \boldsymbol{P_T}$ using "passive polarimeters," where $< \mathbf{B} >$ is the average of muon magnetic field vector. Two independent teams separately carried out careful data analyses and the two results were combined at the end. Thanks to the stopped beam method which enabled a so-called forward (fwd) and backward (bwd) symmetric measurement with regard to the π^0 emission direction (see Fig. 5), and the high rotational symmetric structure of the toroidal spectrometer system, the systematic errors could be substantially suppressed. A full description of the experiment is given in [7]. The final result was

$$P_T = -0.0017 \pm 0.0023\,(stat) \pm 0.0011\,(syst) \tag{16}$$

$$\mathrm{Im}\xi = -0.0053 \pm 0.0071\,(stat) \pm 0.0036\,(syst) \tag{17}$$

corresponding to the upper limits of $|P_T| < 0.0050$ (90% CL) and $|\mathrm{Im}\xi| < 0.016$ (90% CL), respectively. This E246 result was statistics limited, i.e., the total systematic error was less than half of the statistical error. A remarkable point here is that most of the systematic error sources cancelled out after the 12-gap summation due to the rotational symmetry of the system and the fwd–bwd ratio due to its symmetry. The largest error was the effect of

multiple scattering of muons through the Cu degrader of the polarimeter. The J-PARC experiment will be free from this error as we will employ an active polarimeter (see below). There were two items that were not cancelled out by any of the two cancellation mechanisms, the effect from the decay plane rotation, θ_z, and the rotation of the muon magnetic field, δ_z, which might remain as the most serious errors in the J-PARC experiment.

4 J-PARC TREK Experiment

4.1 Goal of the Experiment

Considering the current experimental situation of direct CP violation studies and searches for new physics as discussed in Sect. 2, we believe that it is essential to perform the P_T measurement in $K^+_{\mu 3}$ as the TREK[1] experiment [8] at J-PARC, which offers a far superior experimental environment when compared to KEK-PS. The 40-year history of P_T experiments shows a rather slow improvement in the upper limit. This is due to two reasons: the first point is that the statistical sensitivity of asymmetry measurements scales as $1/\sqrt{N}$ (N is the total number of events), while the single-event sensitivity in rare decay experiments scales as $1/N$. The second reason is the nature of this high-precision experiment which must be conducted and analyzed very carefully. The understanding and reduction of systematic errors can only be achieved step by step. We prefer to follow this approach for the J-PARC experiment and to proceed in a steady way to improve the sensitivity. We plan eventually a long-range strategy to attain the goal of SM+FSI signal region of 10^{-5} in a few steps.

The E246 result was essentially statistics-limited. (The largest systematic error in the error list was due to multiple scattering and was also statistical in nature.) This result was foreseen at the start of the E246 experiment. We propose to improve the E246 result by at least a factor of 20 ($\delta P_T < 1.2 \times 10^{-4}$), by improving both statistical error (by a factor of 20 at least) and systematics uncertainty (by a factor of 10 at least). This sensitivity puts the experiment well into the region where new physics effects can be discovered, and even a null result would set tight constraints on theoretical models. If warranted, further sensitivity improvement toward 10^{-5} will be proposed in the next stage after we have been convinced of the possibility to pursue this experiment to such a high-precision region. In that sense, the TREK experiment may be considered as a prelude to precision frontier experiments at J-PARC.

4.2 Stopped Beam Method

The salient feature of the E246 and TREK experiments is the use of a stopped beam and it was conceptually distinct from the previous BNL-AGS

[1] TREK is an acronym of time reversal experiment with kaons.

experiment [6] where in-flight K^+ decays were adopted for the K^+ decay. The advantages of using decays at rest are briefly summarized below:

- Isotropic decay of K^+ at rest involves all the kinematic conditions covering the full decay phase space. By using a symmetric detector like E246/TREK one can look for the T-odd asymmetry effect in its positive value Dalitz-plot region as well as in its negative region. A double ratio measurement, namely the comparison scheme between forward-going pion events and backward-going pion events was possible. Such a double ratio measurement is essential for high-precision experiments.
- The kinematical resolution is determined in the center-of-mass system in at-rest decays. The energy regions extend up to about 250 MeV and the energies can be easily measured with sufficiently high resolution. Decay particles are detected in the entire 4π sr solid angle region and the relative angles of the particles are measured with good accuracies, limited only by the detector resolutions.
- The isotropic decay at rest with large solid angle coverage ensures that the counting rates are distributed over many segmented detectors, thus keeping the counting rates low enough to minimize the pileup problems. This is an important feature, especially for the electromagnetic calorimeter.
- For a stopped beam experiment, we need not be concerned about the beam history nor the finite emittance of the K^+ beam. The latter is usually large in the case of a low-momentum beam and can cause severe problems in the case of in-flight decay experiments. The kaon stopping distribution is a consequence of the beam emittance in this experiment. The asymmetries in the stopping distributions, however, involve only three parameters of coordinates and they are easy to handle.
- Most parts of the detector are located outside the beam region. Hence, the beam-related pileup effects or background problems are less serious.

In particular, the use of the superconducting toroidal spectrometer setup in the stopped beam experiment offers many advantages.

- The relatively large bending power for charged particles in the field of 0.9 T provides sufficiently good resolution for charged particle analysis. An upgraded charged particle tracking system can make a full use of it.
- The bending of nearly 90° by the sector-type magnet creates a quasi-focal plane with large dispersion at the exit of the magnet. This arrangement effectively prevents most of the background channels such as $K_{\mu 2}$ and $K_{\pi 2}$ from entering the polarimeter.
- The presence of a quasi-focal plane enables a relatively small muon stopping volume when a wedge-shaped momentum degrader is inserted. This is a rather important condition since the relevant momentum range of $K_{\mu 3}$ is wide – 100–200 MeV/c.

The basic analysis in TREK will be done essentially in the following scheme as in the E246 experiment although an extended analysis using all the π^0 region will also be conceivable. The T-odd asymmetry is deduced as

$$A_T = (A_{fwd} - A_{bwd})/2, \tag{18}$$

where the π^0-fwd and bwd asymmetries were calculated using the "clockwise" and "counter-clockwise" positron emission rate N_{cw} and N_{ccw} (red arrows and green arrows in Fig. 5 (left), respectively) as

$$A_{fwd(bwd)} = \frac{N^{cw}_{fwd(bwd)} - N^{ccw}_{fwd(bwd)}}{N^{cw}_{fwd(bwd)} + N^{ccw}_{fwd(bwd)}}. \tag{19}$$

Then, P_T is deduced using the analyzing power α, which is determined by the structure of the polarimeter and its analysis, and the average kinematic attenuation factor $< \cos\theta_T >$, which is determined by the $K_{\mu 3}$ kinematics in the detector, to be

$$P_T = A_T/(\alpha < \cos\theta_T >). \tag{20}$$

Using a conversion coefficient Φ ($\sim$0.3 for a full detector acceptance) calculated in a detector Monte Carlo calculation, the result of Imξ is deduced as

$$\mathrm{Im}\xi = P_T/\Phi. \tag{21}$$

4.3 Upgraded E246 Detector

There are strong arguments which favor performing the experiment in the J-PARC phase 1 with the toroidal spectrometer system by upgrading the E246 detector system.

- The basic performance of the spectrometer is well known to us. Although some upgrades are required in the charged particle tracking, the motion of charged particles in the toroidal magnet is well understood and reproduced well in our simulation calculations. We have carried out, over a period of many years, intensive studies of the CsI(Tl) calorimeter response incorporating its complex geometry of the muon hole and the entrance/exit holes. This system is very well understood.
- The spectrometer magnet and the CsI(Tl) calorimeter are the components that were designed and manufactured with high precision. They were assembled very carefully in order to ensure their performance in a high-precision experiment and have been proven to work without any problem.
- We have full knowledge of the overall performance of the total system including the beam collimation, kaon stopping target, muon slowing-down, and the polarimeter system. For example, we can utilize the existing wedge-shaped muon degrader system which has been well tuned. We know the sources of systematic errors very well and we are able to design the upgrade detector based on the experimental data.
- Finally, the relatively low cost for starting the step 1 experiment as early as possible also favors an upgrade of the E246 detector rather than a new detector.

Also the fact that the beam intensities in the phase 1 of J-PARC will not be very high makes it unnecessary to develop a completely new calorimeter. If we increase the speed of the readout scheme by changing to a faster system based on recent technical developments, we will be able to handle a few times 10^6 per second kaon beam.

Our aim is to perform an experiment which, in comparison to E246, will have about 10 times more acceptance (using active polarimeter described below), about 20 times the integrated beam flux, and a few times higher analyzing power to achieve nearly a factor of at least 20 improvements in the statistical sensitivity, i.e., δP_T (one σ limit) $\sim 10^{-4}$. We feel confident that we can accomplish this task with the modifications described in the next section.

5 TREK Detector

In order to optimize the performance of the toroidal spectrometer system, several improvements must be undertaken. We will keep the principal concept of the experiment, namely the application of the muon magnetic field in the azimuthal direction parallel to the P_T component, and the object of the measurement in this experiment is primarily the *cw–ccw* positron asymmetry in the azimuthal direction, i.e., we keep the fwd/bwd scheme. As for the π^0 detection we cannot use 1γ events anymore since this gives rise to significant background contamination. It is expected that the statistics from the 2γ events only is sufficient to achieve the goal of our experiment in phase 1.

5.1 Active Polarimeter

The most important feature of the TREK experiment is the adoption of an active polarimeter in contrast to E246 where a passive polarimeter with a separate system of a muon stopper and positron counters was used. The advantage of this passive system was the simplicity in the analysis with the consequence of very small systematic errors associated with the analysis. The systematic cancellation scheme when the asymmetry was summed over the 12 sectors was also based on the use of positron counters as clockwise and counter-clockwise counter function at the same time. However, this was done at the cost of e^+ detection acceptance and polarization analyzing power. We now aim for higher detector acceptance and higher sensitivity by introducing the active polarimeter. The suppression of the systematic errors ensured in the E246 passive polarimeter will be guaranteed by a different method. The active polarimeter should have the following functions and advantages.

- An active polarimeter determines the muon stopping position for each event, which in turn renders the experiment free from the systematic error associated with the ambiguities in the muon stopping distribution. As the decay positron tracks are measured, the decay vertices will be determined

event by event. In contrast to the situation in E246, where the positron signal time spectra were associated with non-negligible constant background events, the active polarimeter data will be relatively background free.

- Detection of decay positrons in all directions by a polarimeter with a large acceptance with nearly 4π solid angle. In E246 the positron counter solid angle was limited to about 10% on each side. The detector acceptance becomes 10 times larger, even though the sensitivity does not scale by this factor. The ability to measure positron emission angle provides the possibility to use not only the fwd/bwd pion scheme but also the $left/right$ pion scheme (Fig. 6) which was not possible in E246.
- Measurement of the positron emission angle and rough positron energy by means of the number of penetrating stopper plates. The asymmetry changes as the positron energy varies. A weighted analysis brings about a significant increase in the analyzing power resulting in the highest sensitivity. It is of interest to note that this superior performance is achieved with only moderate energy resolution.

Needless to say the stopper should have a large muon collection/stopping efficiency and the ability to preserve the polarization. In order (1) to ensure preservation of muon spin polarization, in particular the P_T component, and (2) to decouple stray fields such as the earth field, a magnetic field with a strength of at least 300 G is applied at the stopper. As in E246 the azimuthal field arrangement is adopted favoring the fwd/bwd scheme. The muon field magnet produces a uniform field distribution on the stopper.

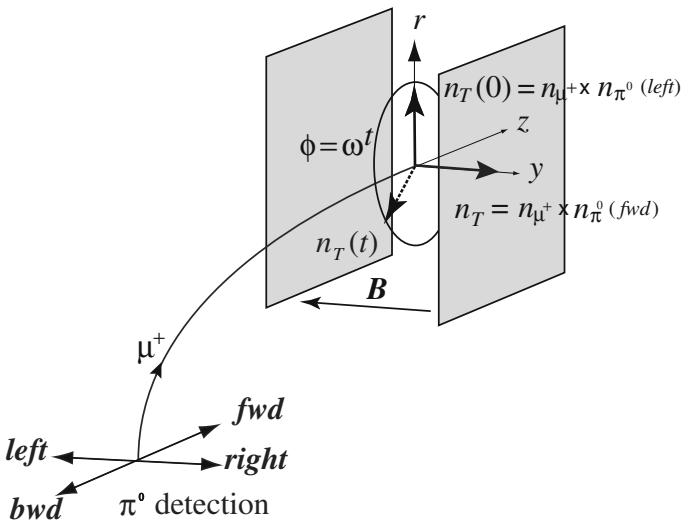

Fig. 6. P_T measurement in the polarimeter. The fwd–bwd scheme and $left$–$right$ scheme are shown.

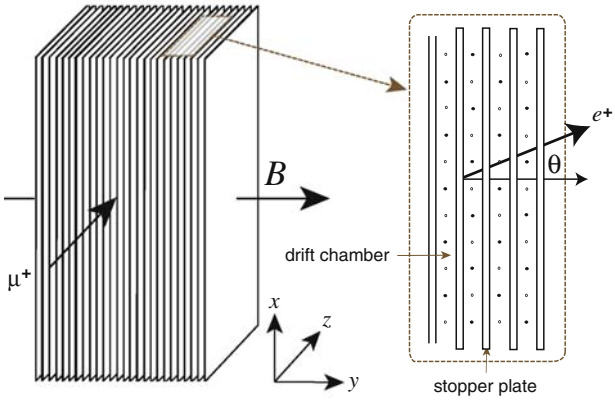

Fig. 7. Schematic view of the active polarimeter with stopper plates and drift chambers.

A parallel plate configuration will be adopted as shown in Fig. 7. The plates are made of light metal (alloy) such as Al or Mg providing the average density of $\sim 1/4\rho_{Al}$. They are arranged in a parallel orientation to the spectrometer gap, namely parallel to the incident muon momentum. Due to the multiple scattering when passing through the Cu degrader in front of the polarimeter, the divergence of the incoming muon beam (in the y direction also) is significant ($\Delta\theta \sim 0.1$) and there is no problem with the muon stopping. A stopping efficiency higher than 0.85 will be obtained. A drift chamber is constructed with these plates as ground potential forming cells with a size of the plate gap. Clearly, this is the best arrangement for the cw/ccw asymmetry measurement, as a single cell acts both as cw cell and a ccw cell for the two neighboring plates. The channel inefficiency cancellation works perfectly.

5.2 Muon Field Magnet

A uniform muon field with a large enough strength is essential in the TREK experiment, whereas a passive field was used by guiding and trimming the main field of the superconducting magnet in E246. The unavoidable consequence was that there was a non-uniform strength distribution and a curved flux distribution at the stopper. A uniform field parallel to the P_T component provides the maximum analyzing power. A new muon field magnet will be made to provide such a field (Fig. 8). To accommodate the polarimeter the parallel gap of the dipole magnet must be about 30 cm. The area is determined to produce a uniform field distribution in the stopper region.

From the point of view of (1) spin relaxation suppression and (2) stray field decoupling, a stronger field is preferable. However, the field is limited by the interference with the toroidal magnet, in particular with its SC coils. Point (2) is regarded as the determining factor; assuming 0.3 G of an unwanted

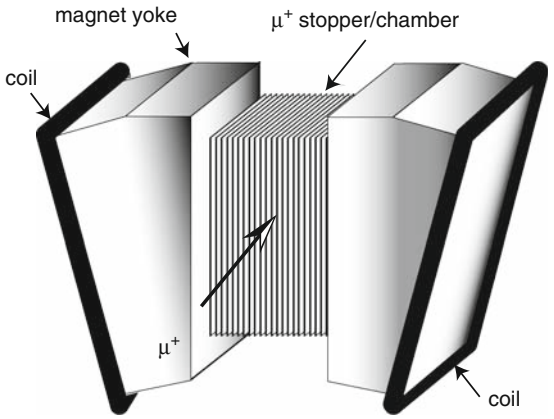

Fig. 8. Schematic view of the muon field magnets sandwiching the active polarimeter.

component in the shielded magnet gap, a field strength of at least 300 G is necessary to obtain a field alignment of 10^{-3}. Further alignment calibration is done by using experimental data.

The field symmetry across the median plane is important but a non-uniformity of a few times of 10^{-2} in strength as well as in the vector distribution is tolerable in the positron energy analysis. A parallel filed arrangement to the SC magnet field rather than the anti-parallel configuration will be selected in order to achieve flatter field uniformity.

5.3 Tracking System

In the TREK experiment two sources of systematic errors will dominate. While one source is the misalignment of the detector elements, in particular of the muon polarimeter, the other source will be given by the background contamination of muons from the decay-in-flight of $K_{\pi 2}$ pions ($K^+_{\pi 2}$-*dif* events). With the upgrade of the tracking system, the error from this background will be improved to meet the requirement of $< 10^{-4}$ for the total systematic error in P_T. These performance goals will be achieved both by reducing the material budget along the track and by rearranging existing and adding new tracking elements in replacement of the previous C1 chamber. The momentum uncertainty of 3.6 MeV/c in E246 can be reduced by at least a factor of 10 (1) by employing a 6-cm- instead of 9.3-cm-wide target with a segmentation of $3.0 \times 3.0\,\mathrm{mm}^2$ fibers instead of $5 \times 5\,\mathrm{mm}^2$, (2) by replacing the air volume in the magnet between C2 and C3 and before the C2 chambers with helium bags, and (3) by increasing the distance between the C3 and C4 elements to 30 cm from 15 cm. For sufficient identification and suppression of $K^+_{\pi 2}$-*dif* events we need to build a cylindrical tracking chamber ("C0") with a radius of 10 cm and a spatial resolution of <0.1 mm. The new C0 chamber will replace the previous

cylindrical C1 chamber of the E246 setup. In order to increase tracking redundancy we propose to add a new planar tracking element (again named "C1") with <0.1 mm resolution to cover each of the 12 gaps at the outer surface of the CsI(Tl) calorimeter. By adding these additional elements to the track fitting procedure, the resulting χ^2 per degree of freedom will be much more effective to distinguish tracks from $K^+_{\pi 2}$-*dif* from regular tracks which do not have a kink along their path. In combination with the higher segmentation of the fiber target this will be sufficient to suppress the $K^+_{\pi 2}$-*dif* $/K^+_{\mu 3}$ ratio below 10^{-3}, rendering a spurious $P_T < 5 \times 10^{-5}$.

The planned modifications are in summary:

(1) Thinner target with higher segmentation.
(2) Helium gas bags in the magnet between C2 and C3, and before C2.
(3) Increase in the distance between C3 and C4 to 30 cm from 15 cm.
(4) Addition of new tracking elements: "C0" and "C1" chambers based on GEM technology.

Figure 9 and Table 4 show comparisons of the tracking system in E246 and the TREK experiment. The GEM technology on which both C0 and C1 will be based presents a new generation of position-sensitive counters that are reasonably cheap, radiation hard, and well suited to be operated in high-rate environments.

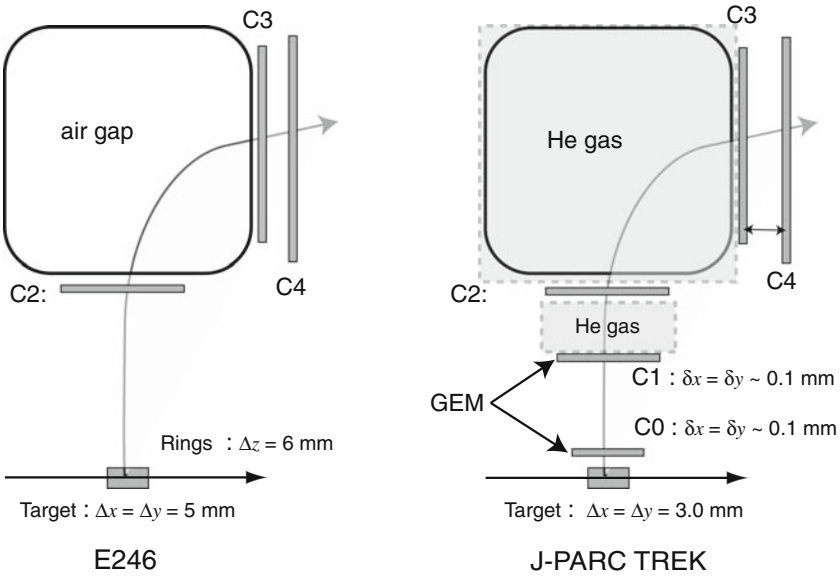

Fig. 9. Schematics of the tracking system in the TREK setup (*right*) compared with that of the E246 experiment (*left*).

Table 4. Main parameters of the charged particle tracking.

Item	Value	E246
High-resolution elements	C0, C1, C2, C3, and C4	C2, C3, and C4
Target fiber	3×3 mm	5×5 mm + rings
C0 chamber	Cylindrical GEM	MWDC
C1 chamber	Planar GEM chamber	–
C2 chamber	MWPC (not changed)	MWPC
C3 chamber	MWPC (not changed)	MWPC
C4 chamber	MWPC (not changed)	MWPC
C3–C4 distance	30 cm	15 cm
Magnet gap	He gas bag	Air
Total material thickness	$\sim 7 \times 10^{-3} X_0$	$6.6 \times 10^{-3} X_0$

5.4 CsI(Tl) Calorimeter

The photon calorimeter is a barrel of 768 CsI(Tl) crystals surrounding the target region (Fig. 10). There are 12 so-called muon holes to let the charged particle enter the spectrometer. The solid angle coverage is therefore not 4π sr but about 3π sr including also the losses due to the beam entrance and exit holes. The size of the muon hole was optimized for the $K^+_{\mu 3}$ acceptance to be maximum [51]. The barrel structure is symmetric for the upstream (backward) and the downstream (forward) side, which is essential in the present experiment. The barrel was assembled very carefully ensuring a local as well as a global precision of better than 1 mm. The main parameters of the barrel are summarized in Table 5.

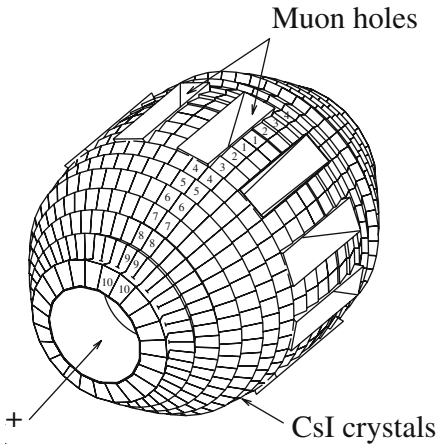

Fig. 10. CsI(Tl) barrel with 768 crystal modules. There are 12 muon holes.

Table 5. Main parameters of the CsI(Tl) calorimeter.

Parameter	Value
Number of CsI(Tl) crystals	768
Segmentation	$\Delta\theta = \Delta\phi = 7.5^\circ$
Inner/outer diameter	41/90 cm
Detector length	141 cm
Solid angle coverage	∼75%
Crystal length	25 cm (13.5 X_0)
Typical size of crystals	$3 \times 3 - 6 \times 6$ cm^2
Wavelength at peak	560 nm
Light decay time	∼900 ns

Considering the limitations in the PIN + preamplifier scheme for high-rate operation, we plan to adopt another CsI(Tl) readout method. One possibility is to use magnetic field-resistant photo-multiplier tubes now available with fairly large multiplication. However, the space limitation will still be a problem. There is also a cost question. Thus, we are led to consider avalanche photo-diodes (APD) of reverse bias type. Such APDs with a multiplication factor of about 100 with reasonably large sensitive areas are commercially available [54]. Several applications to calorimeters in high-energy physics experiments are being prepared. The wavelength matching to CsI(Tl) with the peak wavelength of 560 nm is better than PWO[55] and an average quantum efficiency greater than 80% can be expected. The readout of CsI(Tl) by an APD has already been studied in Ref. [56] by using Hamamatsu S8664 for a small crystal and it was found to work well.

A several times larger electron yield than the PIN (E246) with 5×10^6/100 MeV allows us to use a current preamplifier with high gain in place of the costly charge preamplifier which would also encounter the rate limitation due to the output voltage dynamic range. A high-rate performance test of APD readout has been performed using a positron beam for one crystal module with a prototype amplifier for S8664. About 500 kHz signal rate in one module will be tolerable and analyzable using an FADC (Table 6).

5.5 Alignments

Since the misalignments of detector elements may cause systematic errors, precise alignment is essential in the TREK experiment. The alignment of the tracking system and the CsI(Tl) calorimeter system relative to the reference system of the spectrometer will be performed using a set of calibration collimators for the former and $K_{\pi 2}$ events for the latter. Although careful designs are required for both, we regard the calibration procedure to be rather straightforward; the performance of the calibration can be easily checked with simulations. They are all fwd/bwd cancelling and thus controllable. On the

Table 6. Readout scheme using APDs compared with the E246 PIN readout.

Parameter	E246-PIN	APD readout
Diode	S3204-03	S8148 (or equiv.)
Total area	$18\times18\,\mathrm{mm}^2$	$5\times5\,\mathrm{mm}^2$
Quantum efficiency	$\sim$0.70	> 0.80
Photoelectron/GeV	1.1×10^7	1.0×10^6
Diode gain	1	50
Electron yield@ 100 MeV	1.1×10^6	5.0×10^6
Preamplifier	Charge sensitive	Current amplifier
Maximum rate	34 kHz	$\sim$500 kHz

contrary, the effect of polarimeter misalignments, which are direct systematics affecting the positron asymmetry, $A_{fwd(bwd)}$, is complicated with the entanglement of several factors including the muon field. Moreover, one of the misalignments, the rotation of the muon field around the z-axis δ_z, is the systematics which cannot be canceled out in the normal π^0 fwd/bwd subtraction scheme. In the following we present the alignment method of the polarimeter, which we regard as the most important in this experiment.

The misalignment of the polarimeter is characterized by four parameters: global rotation of the active stopper (1) around the r-axis, ϵ_r-and (2) around the z-axis, ϵ_z, and global rotation of the muon field distribution (3) around the r-axis, δ_r, and (4) around the z-axis, δ_z. They are only responsible for spurious $A_{fwd(bwd)}$; parallel displacements should not play a role as long as the active stopper covers the whole muon stopping region because of the parallel-shift symmetric structure. The rotation about the y-axis should not have any effect since it brings about only a rotation around the azimuthal axis.

In order to treat this problem an innovative method [57] will be performed using $K_{\mu3}$ data so as to remove any misalignment effects from the P_T analysis. The time integrated e^+ left/right asymmetry $\bar{A}$ due to the misalignments can be described for a certain initial muon spin phase in the median planes θ_0 measured from the direction of z beam axis as follows:

$$\bar{A}\,(\theta_0) = \alpha_0[\delta_r \cos\theta_0 - \delta_z \sin\theta_0 + \eta\,(\theta_0)], \tag{22}$$

where α_0 is the analyzing power for the polarization determination from the e^+ asymmetry. The oscillation terms with ωt are drastically reduced by the time integration and the remaining imperfect cancellation is expressed as $\eta(\theta_0)$. It is noted that the misalignments of the active stopper were integrated out into $\eta(\theta_0)$ and hence they are not relevant in the further discussion.

To extract the misalignment parameters δ_r and δ_z in the presence of a real P_T signal, we calculate two asymmetries A_{sum} and A_{sub} as a function of θ_0, i.e., the sum and difference of A_{fwd} and A_{bwd} – the asymmetries at the forward and backward pions, respectively. This leads to

$$A_{sum}(\theta_0) = \left[\bar{A}_{fwd}(\theta_0) + \bar{A}_{bwd}(\theta_0)\right]/2 \cong \alpha_0 \left[\delta_r \cos\theta_0 - \delta_z \sin\theta_0\right], \quad (23a)$$

$$A_{sub}(\theta_0) = \left[\bar{A}_{fwd}(\theta_0) - \bar{A}_{bwd}(\theta_0)\right]/2 = F(P_T, \theta_0), \quad (23b)$$

where $F(P_T, \theta_0)$ is the A_T asymmetry function only from a P_T origin and it does not involve any misalignment effects. Thus, we can extract P_T from $F(P_T, \theta_0)$ unaffected by the misalignments.

The validity of this method must be demonstrated with an MC calculation with high statistics. This MC study should show a unique determination of the misalignments when several misalignments are existing simultaneously and to check for any bias in the analysis including a possible bias in the tracking code. Assuming the existence of both δ_z and δ_r but no P_T, the A_{sub} analysis was performed using 25 billion events of $K_{\mu 3}$ decays, and P_{sub}^{av} was obtained from the averaged A_{sub} to be $P_{sub}^{av} = \alpha_0 A_{sub}^{av} = (0.3 \pm 0.6) \times 10^{-4}$. The result, which is consistent with zero within the statistical error, indicates the appropriateness of this analysis including the absence of any bias in the analysis code.

5.6 Beamline

In order to perform the TREK experiment using stopped K^+s, a separate low-momentum K^+ beamline with a good K/π ratio is required. In the phase 1 experimental hall of J-PARC, however, there will be only one primary proton line, A-line, and only one target station T1. All the secondary lines are going to be installed at this target. The construction of the beam facility is now proceeding according to the policy to accommodate the nuclear physics experiments which were nominated as "day-1 experiments." Thus, the K1.8 and K1.1 lines are most likely to be built first, and the structure of the target station and the front end of the channels are now almost fixed. Considering the high-current operation of the facility, those designs with a very limited channel acceptance seem to be unique, and it will be difficult to modify the structure after starting a full-intensity operation. Even under such a situation, we pursue the possibility of a low-momentum beamline K0.8 with a beam momentum of 0.8 GeV/c which is optimum for the planned experiment. We have found a good solution, which is a branch line of the K1.1 line, and it can provide a high-quality low-momentum beam with a sufficiently good K/π ratio. The beam optics of this branch have been designed.

The quality of the 0.8 GeV/c separated kaon beam at this branch line, with a single stage of separation with a K^+/π^+ ratio larger than 2, is very good for our purposes. This is achieved by the existence of a vertical focus and also by the horizontal focus additionally designed for the K0.8 branch. The acceptance of K0.8 is, however, determined primarily by the upstream acceptance of K1.1, namely by the distance of the first focusing element from the target, which cannot be shorter. The calculated acceptance of ∼4.5 msr(%$\Delta p/p$) is smaller by a factor of 10 than the C4 (LESB3) line at BNL-AGS of the nearly same length for 0.8 GeV/c operation. Although there might be some ambiguity due

Table 7. Main parameters of the K0.8 beam.

Parameter	Value
Momentum	800 MeV/c
Momentum bite	±2.5%
Channel length	19 m
Channel acceptance	4.5 msr%($\Delta p/p$)
π^+/K^+ ratio	< 0.5
K^+ intensity	3×10^6 @ 9 μA proton beam
Beam spot	$H = \pm 0.3$ (FWHM) cm, $V = \pm 0.4$ (FWHM) cm $H = \pm 1.6$ (total) cm, $V = \pm 1.6$ (total) cm
Dispersion at final focus	Achromatic

to the detailed target structure, we can roughly estimate the K^+ intensity to be 2×10^6/s at $I_p = 5.4 \times 10^{13}$/s (9 μA) and $E_p = 30$ GeV by scaling the known LESB3 intensity at $E_p = 24$ GeV. The main parameters of K0.8 are summarized in Table 7.

6 Sensitivity

6.1 Statistical Sensitivity

For a conservative estimate we assume the sensitivity coefficient for the integral analysis taking the *fwd* and *bwd* regions of the π^0 events. Several comments are presented for the other parameters.

1. The average beam intensity at the K0.8 beamline is assumed to be 2×10^6/s. Although it is stated that some beam commissioning period with a low accelerator beam intensity is necessary, our total beam request is 1.4×10^7 s of beam time with this kaon beam intensity. We estimate the sensitivity based on the total number of kaons of 3×10^{13}.
2. The fraction of *fwd* and *bwd* regions is 30% of the total good $K_{\mu 3}$ events including the *left* and *right* regions. It is somewhat difficult to estimate the analysis efficiency as it strongly depends on many details. However, at least for now, we can assume that it would be better than what we attained in E246. We use a conservative estimate of 0.67, the E246 efficiency.

The deduction of the statistical error is summarized in Table 8. In the standard *fwd/bwd* π^0 analysis a statistical error of $\delta P_T = 1.2 \times 10^{-4}$ will be obtained from a 1-year (1.4×10^7 s) run. An analysis including the *left* and *right* regions will provide a smaller error of $\delta P_T = 1.0 \times 10^{-4}$. A more ambitious weighted analysis event by event should attain the highest sensitivity of $\delta P_T = 0.8 \times 10^{-4}$ although the systematic errors have yet to be investigated carefully in this case.

Table 8. Deduction of statistical error.

Parameter	Value
Net runtime	1.4×10^7s
Proton beam intensity	9 μA on T1 target
K^+ beam intensity	2×10^6/s
Total number of good $K_{\mu 3}$	2.4×10^9
Total number of fwd and bwd (N)	7.2×10^8
Sensitivity coefficient	$3.34/\sqrt{N}$
δP_T for fwd and bwd	1.2×10^{-4}
δP_T for all π^0	1.0×10^{-4}
δP_T in weighted analysis	0.8×10^{-4}

6.2 Systematic Errors

As mentioned before the main sources of systematic errors in E246 must be suppressed substantially at least by 1 order of magnitude. The following summary observations are in order:

- The effects of polarimeter misalignments, in particular the field rotation δ_z, are not more relevant to the P_T determination. If necessary, they can be calibrated using data. Monte Carlo simulation studies assuming considerably large misalignments for the rotation parameters ϵ_r, ϵ_z, δ_r, and δ_z showed the associated systematic error to be smaller than 10^{-4} in the discrepancy between the fit value and the input value.
- The influence of decay phase space distortion parameterized by the decay plane angular parameters θ_r and θ_z should be corrected. The error associated with these corrections is essentially a statistical one and is estimated to be far less than 10^{-4} for both θ_r and θ_z. The validity of the correction method can be checked by introducing an artificial asymmetry in, for example, the kaon stopping distribution in the target to produce significant θ_r and θ_z.
- The error due to $K^+_{\pi 2}$-dif background contamination can be suppressed by means of the new upgraded tracking system down to less than 5×10^{-5}.
- There is a new potential source of error which was not present in E246, namely the error coming from the active polarimeter analysis. Although the detailed design of the polarimeter has yet to be done, the effects of E_{e^+} and θ_{e^+} ambiguities have to be suppressed to the level smaller than 10^{-4}.
- The largest systematic error in E246, which was the ambiguity of muon stopping point due to scattering, does not exist in the TREK polarimeter anymore.

Other potential sources such as the misalignments of the tracking elements are regarded as rather harmless since the correction based on the alignment calibration can be done accurately enough. Although the necessary Monte

Table 9. Expectation of the systematic errors in E06.

Source	$\delta P_T^{syst}(10^{-4})$	Method
Polarimeter misalignment ($\delta_z, \delta_r, \epsilon_z$, and ϵ_r)	<1	Confirmed by MC simulation
$K_{\pi 2}$-dif background	$\ll 0.5$	Confirmed by MC simulation
Decay plane rotations (θ_z and θ_r)	$\ll 1$	Correction and data symmetrization
Positron analysis (E_{e^+} and θ_{e^+})	<1	Fwd/bwd cancellation, fwd/bwd symmetrization, etc.
Total	$\delta P_T^{syst} \preceq 10^{-4}$	Quadratic sum

Carlo studies will be continued we believe that each correction is applied with an uncertainty of less than 10% of the correction values and that the total systematic error can be made much smaller than 10^{-4}. These expectations are summarized in Table 9.

7 Summary

In summary, we plan to perform a high-precision measurement (TREK experiment) of the transverse polarization of muons in the $K^+_{\mu 3}$ decays, which constitutes a T-odd observable. This observable is one of the few tests of T-invariance corresponding to direct CP violation in non-neutral meson system. We aim to improve the precision of this measurement at least by a factor of 20 compared to the best result from our own KEK-PS-E246 and reach a limit of $\delta P_T \sim 10^{-4}$ (Fig. 11). The FSI contribution in the SM descriptions is significantly smaller than the sensitivity of this type of measurement; however, several exotic models inspired by multi-Higgs doublet, etc., allow P_T values within the sensitivity attainable to us. Thus, this experiment is likely to find new sources of CP violation, if any of these models are viable. It will certainly constrain the parameter space of the candidate models. The sensitivity of this experiment is comparable or complementary to that of the proposed new neutron EDM experiments and other rare decay processes, since P_T as a semi-leptonic process spans the parameter space which is not covered by other channels.

The experiment will be performed using the stopped K^+ beam method as the previous KEK-E246 experiment. This method is suited for a double ratio measurement in terms of π^0 emission direction, enabling the efficient suppression of systematic errors, which is essential for the high-precision experiment TREK. Although the basic toroidal setup of E246 is used, several upgrades of the detector element will be done in order to meet the requirements from higher rate performance, larger acceptance, better background rejection, and more efficient suppression of the systematic errors. The major upgrades are as follows:

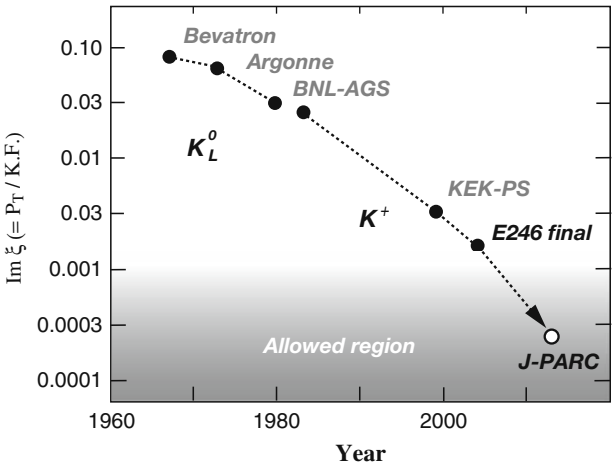

Fig. 11. Expected sensitivity (90% CL assuming a zero central value) of the TREK experiment.

- Adoption of active polarimeters to ensure the small systematic error, higher analyzing power using the energy and angle information of emitted positrons, and larger acceptance of nearly 4π. The decay positron measurement will be background free.
- Improvement of the charged particle tracking system by additional tracking elements using state-of-the-art GEM detectors for the innermost two detectors, C0 and C1. Together with a slimmer target with finer segmentation the new system can suppress the $K^+_{\pi 2}$-*dif* background drastically.
- Faster readout of the CsI(Tl) calorimeter by means of APD and FADC. The rate capability will be more than 10 times higher.
- Alignment of the detector elements with high precision. Especially, the global alignment of the polarimeter and the muon field which are the most serious systematics affecting the positron asymmetry will be done using real data as one of the processes to deduce P_T.

We are now planning to perform the TREK experiment in the early stage of the phase 1 period of J-PARC. The high-quality beam from the K0.8 beamline and the upgraded high-precision detector will enable us to attain the sensitivity of $\delta P_T \sim 10^{-4}$ in a 1-year run of the measurement.

Acknowledgments

The author would like to thank all the members of the TREK collaboration for valuable discussions. He would also like to acknowledge the discussions with the J-PARC hadron facility group on the beamline.

References

1. Bigi, I.I., Sanda, A.I.: CP Violation. Cambridge University Press (2000) 75, 79, 80
2. See, for example, Prologue of [1] 75
3. Sakurai, J.J.: Phys. Rev. **109**, 980 (1957) 75
4. Zhitnitkii, A.R.: Yad. Fiz. **31**, 1014 (1980) 75, 79
5. Efrosinin, V.P., et al.: Phys. Lett. **B493**, 293 (2000) 75, 79
6. Blatt, S.R., et al.: Phys. Rev. **D27**, 1056 (1983) 75, 84, 88
7. Abe, M., et al.: Phys. Rev. **D73**, 072005 (2006) 76, 84, 86
8. J-PARC proposal P06; Measurement of T-violating Muon Polarization in $\boldsymbol{K^+ \to \pi^0 \mu^+ \nu}$ Decays. http://j-parc.jp/NuclPart/Proposal e.html (2006) 76, 81, 87
9. Cabibbo, N., Maksymowicz, A.: Phys. Lett. **9**, 352 (1964) 76, 77
10. Cabibbo, N., Maksymowicz, A.: Phys. Lett. **11**, 360(E) (1964)
11. Cabibbo, N., Maksymowicz, A.: Phys. Lett. **14**, 72(E) (1966)
12. Eidelman, S. et al.: [Particle Data Group], p.618 in "Review of Particle Physics". Phys. Lett. **B592**, 1 (2004) 76, 77
13. Wu, G.-H., Kiers, K., Ng, J.N.: Phys. Rev. **D56**, 5413 (1997) 78
14. Kobayashi, M., Lin, T.-T., Okada, Y.: Prog. Theor. Phys. **95**, 361 (1995) 78
15. Leurer, M.: Phys. Rev. Lett. **62**, 1967 (1989) 78
16. Golowich, E., Valencia, G.: Phys. Rev. **D40**, 112 (1989) 79
17. Harris, P. [EDM collaboration]: Preliminary result presented at SUSY-2005, Durham, June 2005 79, 81
18. Graham, M.: Talk given at "Flavor Physics and CP Violation", Vancouver, April 9–12, 2006 79
19. Ahn, J.K. et al.: Phys. Rev. Lett. **100**, 201802 (2008) 80
20. Particle Data Group: Review of particle physics, J. Phys. G: Nucl. Part. Phys. **33**,1, 688 (2006) 80
21. Garisto, R., Kane, G.: Phys. Rev. **D44**, 2038 (1991) 80, 81
22. Bélanger, G., Geng, C.Q.: Phys. Rev. **D44**, 2789 (1991) 80, 81
23. Sanda, A.I., Phys. Rev. **D23**, 2647 (1981)
24. Deshpande, N.G.: Phys. Rev. **D23**, 2654 (1981)
25. Cheng, H.-Y.: Phys. Rev. **D26**, 143 (1982)
26. Cheng, H.-Y.: Phys. Rev. **D34**, 1397 (1986)
27. Bigi, I.I., Sanda, A.I.: Phys. Rev. Lett. **58**, 1604 (1987)
28. Leurer, M.: Phys. Rev. Lett. **62**, 1967 (1989)
29. H.-Cheng, Y.: Phys. Rev. **D42**, 2329 (1990) 81
30. Grossman, Y.: Int. Mod, J. Phys. **A19**, 907 (2004) 81
31. Hurth, T.: Rev. Mod. Phys. **75**, 1159 (2003) 81
32. Ikado, K., et al. (Belle collaboration): Phys. Rev. Lett. **97**, 251802 (2006) 81
33. Grossman, Y.: Nucl. Phys. **B426**, 355 (1994) 81
34. Okada, Y., Shimizu, Y., Tanaka, M.: arXiv:hep-pf/9704223 81
35. Wu, G.-H., Ng, J.N.: Phys. Lett. **B392**, 93 (1997) 82
36. Fabbrichesi, M., Vissani, F.: Phys. Rev. **D55**, 5334 (1997) 83
37. Christova, E., Fabbrichesi, M.: Phys. Lett. **B315**, 113 (1993) 83
38. Dreiner H.: An introduction to explicit R-parity violation. In: Kane, G.L. (ed.) Perspectives on Supersymmetry (1998) 83
39. Chen, S.-L. et al.: JHEP **09**, 044 (2007); http://jhep.sissa.it/archive/papers/jhep092007044/jhep092007044.pdf 83
40. Barbier R., et al.: Phys. Rept. **420**, 1 (2005); [hep-ph/0406039] 83

41. Chemtob, M.: Prog. Part. Nucl. Phys. **54**, 71 (2005); [arXiv:hep-ph/0406029 2 June 2008] 83
42. Deandrea, A., et al.: JHEP **10**, 038(2004); [arXiv:hep-ph/0407216v2 20 Oct 2004] 83
43. Young, K., et al.: Phys. Rev. Lett. **18**, 806 (1967) 84
44. Longo, J.J., Ypung, K.K., Helland, J.A.: Phys. Rev. **181**, 1808 (1969) 84
45. Sandweiss, J. et al.: Phys. Rev. Lett. **30**, 1002 (1973) 84
46. Morse, W. M. et al.: Phys. Rev. **D21**, 1750 (1980) 84
47. Tanaka, K.H. et al.: Nucl. Instrum. Methods Phys, Res. Sect. **A363**, 114 (1995) 84
48. Imazato, J., et al.: Proc. 11th Int. Conf. on Magnet Technology, Tsukuba, Japan, August 1989 84
49. Ikeda, T., et al.: Nucl. Instr. Meth. Phys. Res. Sect. **A401**, 243 (1997) 84
50. Macdonald, J.A. et al.: Nucl. Instrum. Meth. Phys. Res. Sect. **A506**, 60 (2003) 86
51. Dementyev, D.V. et al.: Nucl. Instrum. Meth. Phys. Res. Sect. **A440**, 15 (2000) 86, 95
52. Yu. G., Kudenko, et al.: Nucl. Instr. Meth. Phys. Res. Sect. **A411**, 437 (1998) 86
53. Ivashkin, A.P., et al.: Nucl. Instrum. Meth. Phys. Res. Sect. **A394**, 321 (1997) 86
54. Hamamatsu Photonics K.K.: Technical Information SD-28, Oct, 2001; Cat. No. KAPD1012J02, April, 2004 96
55. Britvitch, I., et al.: Nucl. Instrum. Meth. Phys. Res. Sect. **A535**, 523 (2004) 96
56. Ikagawa, T. et al.: Nucl. Instrum. Meth. Phys. Res. Sect. **A538**, 640 (2005) 96
57. Shimizu, S.: Proceedings of the Kaon International Conference 2007, Frascatti (2007), http://pos.sissa.it//archive/conferences/046/025/KAON 025.pdf 97